Supplementary Material for

Irremovable Mn-Bi Site Mixing in $MnBi_2Te_4$

Xi Wu[1,4], Chao Ruan[1], Peizhe Tang[2,3], Feiyu Kang[1], Wenhui Duan[4,5,6], and Jia Li[1]*

[1]Shenzhen Geim Graphene Center and Institute of Materials Research, Shenzhen International Graduate School, Tsinghua University, Shenzhen 518055, China

[2]School of Materials Science and Engineering, Beihang University, Beijing 100191, China

[3]Max Planck Institute for the Structure and Dynamics of Matter and Center for Free Electron Laser Science, Hamburg 22761, Germany

[4]State Key Laboratory of Low Dimensional Quantum Physics and Department of Physics, Tsinghua University, Beijing 100084, China

[5]Institute for Advanced Study, Tsinghua University, Beijing 100084, China

[6]Frontier Science Center for Quantum Information, Beijing100084, China

[*]Corresponding author: J. L. (li.jia@sz.tsinghua.edu.cn)

Section I. Computational Methods

Spin-polarized density functional theory (DFT) calculations were performed as implemented in the Vienna *Ab-initio* Simulation Package (VASP)[1]. The electron-ion interaction and the exchange-correlation energy were described by the projected augmented wave method[2,3] and the generalized gradient approximation (GGA) with the Perdew-Burke-Ernzerhof (PBE) functional[4]. The energy cutoff for the plane-wave basis expansion was set to 300 eV for structure optimization and 350 eV for electronic structure calculations. The localized *d*-orbital of Mn was treated by the GGA+U method[5] with an effective U of 4 eV based on previous studies[6,7]. The van der Waals interaction between the layers of $MnBi_2Te_4$ was treated by the empirical correction DFT-D3 method[8]. To simulate the phase transition, the 4 × 4 × 1 supercell of $MnTe/Bi_2Te_3$ monolayer and $MnBi_2Te_4$ monolayer was constructed to study the exchange of Mn-Bi pairs. The structure optimization was performed with a Γ-centered 2 × 2 × 1 *k*-grid mesh, the energy convergence of 10^{-5} eV, and the residual force convergence of 0.01 eV/Å per atom. The kinetic barrier was evaluated by the climbing image nudged elastic band (CI-NEB) method[9]. For the perfect $MnTe/Bi_2Te_3$ and $MnBi_2Te_4$ monolayers, the band structures with or without spin-orbit coupling (SOC) were calculated using the primitive unit cell with a Γ-centered 13 × 13 × 1 *k*-grid mesh. For the intermediates during the phase transition, the 4 × 4 × 1 supercell was selected to calculate the band structures with a Γ-centered 3 × 3 × 1 *k*-grid mesh. For the sake of comparison, the band structures of these intermediates were unfolded to the unit cell. Due to limited computational resources, the unfolded band structures of these supercells were considered without the SOC.

Section II. Formation energy of point defects in the $MnTe/Bi_2Te_3$ and $MnBi_2Te_4$ monolayer

The formation energy of point defects can be calculated using the following equation

$$E_f = E_{def} - E_{per} - \sum n_i \mu_i \quad (1)$$

where E_{def} and E_{per} refer to the total energy of the cells with and without the defects, respectively, n_i refers to the difference in the number of *i*th atomic species between the defect-containing and defect-free cells, and μ_i refers to the chemical potential of the *i*th atomic species. According to **Eq. (1)**, the stability of the point defects is determined by the chemical potential of the atomic species in the target product. However, the chemical potentials of the atomic species in its bulk phase are selected as the chemical potentials of the atomic species under the rich condition. Therefore, $\Delta\mu_i$ is introduced in **Fig. S1** as the relative chemical potential of the *i*th atomic species with respect to the chemical potential of its bulk phase ($\Delta\mu_i = \mu_i - \mu_{bulk}$) to adjust their chemical potentials under the rich condition to zero.

In order to calculate the formation energy of point defects in $MnBi_2Te_4$, the stable region of $MnBi_2Te_4$ in the phase diagram formed by the chemical potentials of Mn, Bi, and Te should be determined first. During the synthesis of $MnBi_2Te_4$, we should maintain its stability and avoid the formation of by-products, such as elementary substances, including Mn, Bi, and Te, or binary substances, including MnTe, $MnTe_2$, BiTe, Bi_4Te_3, Bi_2Te_3, Bi_8Te_9, and Mn-Bi alloy. In order to maintain the stability of $MnBi_2Te_4$, the chemical potentials of Mn, Bi, and Te should satisfy the following equation,

$$\mu_{\mathrm{Mn}} + 2\mu_{\mathrm{Bi}} + 4\mu_{\mathrm{Te}} = \Delta H(\mathrm{MnBi_2Te_4}) \quad (2)$$

where μ_{Mn}, μ_{Bi}, and μ_{Te} refer to the relative chemical potentials of Mn, Bi, and Te, respectively, which are independent of each other, and $\Delta H(\mathrm{MnBi_2Te_4})$ refers to the enthalpy of $MnBi_2Te_4$. To avoid the formation of the by-products, the chemical potentials of Mn, Bi, and Te should satisfy the following inequalities,

$$\mu_{\mathrm{Mn}} \leq 0 \quad (3)$$

$$\mu_{\mathrm{Bi}} \leq 0 \quad (4)$$

$$\mu_{\mathrm{Te}} \leq 0 \quad (5)$$

$$\mu_{\mathrm{Mn}} + \mu_{\mathrm{Te}} \leq \Delta H(\mathrm{MnTe}) \quad (6)$$

$$\mu_{\mathrm{Mn}} + 2\mu_{\mathrm{Te}} \leq \Delta H(\mathrm{MnTe_2}) \quad (7)$$

$$\mu_{\mathrm{Bi}} + \mu_{\mathrm{Te}} \leq \Delta H(\mathrm{BiTe}) \quad (8)$$

$$4\mu_{\mathrm{Bi}} + 3\mu_{\mathrm{Te}} \leq \Delta H(\mathrm{Bi_4Te_3}) \quad (9)$$

$$2\mu_{\mathrm{Bi}} + 3\mu_{\mathrm{Te}} \leq \Delta H(\mathrm{Bi_2Te_3}) \quad (10)$$

$$8\mu_{\mathrm{Bi}} + 7\mu_{\mathrm{Te}} \leq \Delta H(\mathrm{Bi_8Te_7}) \quad (11)$$

$$8\mu_{\mathrm{Bi}} + 9\mu_{\mathrm{Te}} \leq \Delta H(\mathrm{Bi_8Te_9}) \quad (12)$$

where $\Delta H(\mathrm{MnTe})$, $\Delta H(\mathrm{MnTe_2})$, $\Delta H(\mathrm{BiTe})$, $\Delta H(\mathrm{Bi_4Te_3})$, $\Delta H(\mathrm{Bi_2Te_3})$, $\Delta H(\mathrm{Bi_8Te_7})$, and $\Delta H(\mathrm{Bi_8Te_9})$ refer to the enthalpies of MnTe, $MnTe_2$, BiTe, Bi_4Te_3, Bi_2Te_3, Bi_8Te_7, and Bi_8Te_9, respectively. The inequality that avoids the formation of the Mn-Bi alloy is not listed because the stable region of the Mn-Bi alloy is not within the region constructed by **Eq. (2)**.

The stable region satisfying the above equation and inequalities is shown in **Fig. S1**, which is comparable to previous results[10,11]. The stable phase of $MnBi_2Te_4$ is bounded by MnTe, $MnTe_2$, BiTe, and Bi_2Te_3 phases, which is represented by a segment between A and B in **Fig. S1**, indicating that the enthalpy change for the formation of $MnBi_2Te_4$ phase from MnTe and Bi_2Te_3 phases is close to zero.

In the experiment, $MnBi_2Te_4$ sample is always annealed in a protective atmosphere of Te to improve its quality, so the chemical potential of Te from poor to rich condition is chosen to represent the variety of environments during annealing. All the formation energies of point defects in $MnTe/Bi_2Te_3$ and $MnBi_2Te_4$ monolayers are calculated within the range of $\Delta\mu_{\mathrm{Te}}$, which is obtained by the stable region of $MnBi_2Te_4$. In addition, the point defects in $MnTe/Bi_2Te_3$ monolayer with a higher formation energy above 1.0 eV are summarized in **Fig. S2**.

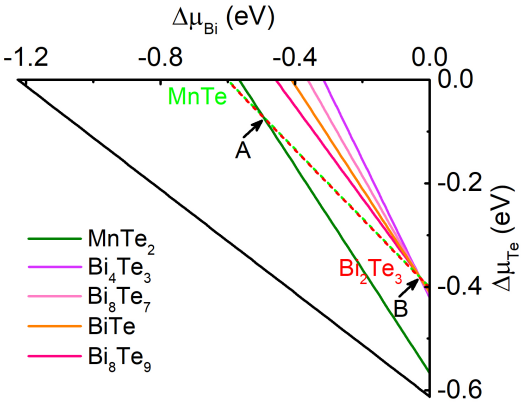

Figure S1. Phase diagram for the formation of $MnBi_2Te_4$ with chemical potentials of Mn, Bi, and Te.

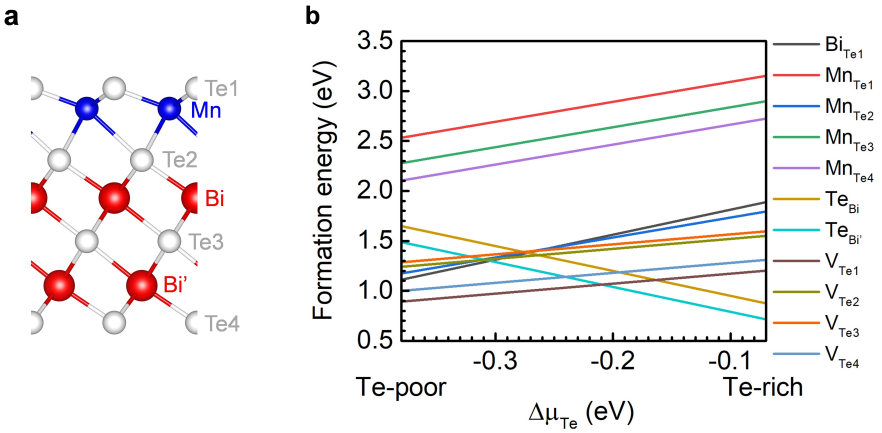

Figure S2. Point defects in the $MnTe/Bi_2Te_3$ monolayer. a Atomic structure of the $MnTe/Bi_2Te_3$ monolayer. **b** Formation energy of different point defects in the $MnTe/Bi_2Te_3$ monolayer.

Section III. CI-NEB calculation of Mn-Bi pair exchange during the phase transition from the $MnTe/Bi_2Te_3$ to $MnBi_2Te_4$ monolayer

To simulate the phase transition from the $MnTe/Bi_2Te_3$ to $MnBi_2Te_4$ monolayer, a $4 \times 4 \times 1$ supercell is constructed to study the Mn-Bi pair exchange. A total of sixteen Mn-Bi pairs should be exchanged to complete the phase transition in our model. Here, the phase transition from the $MnTe/Bi_2Te_3$ to $MnBi_2Te_4$ monolayer would generally pass through three stages, initial, intermediate, and final. And the initial, intermediate, and final stages refer to no or few, about half, and almost all Mn-Bi pairs being exchanged, respectively. In the initial stage, the perfect $MnTe/Bi_2Te_3$ monolayer without any exchanged Mn-Bi pair (I0) and with one exchanged Mn-Bi pair (I1) are chosen as the initial state (IS) and final state (FS), respectively. As shown in **Fig. S3a**, a transition state (TS) with an energy barrier of 2.44 eV is identified. In the intermediate stage, the $MnTe/Bi_2Te_3$ monolayer with eight exchanged Mn-Bi pairs (M8) and with nine exchanged Mn-Bi pairs (M9) are chosen as IS and FS, respectively, with the kinetic barrier of 1.79 eV (**Fig. S3b**). In the final stage, the $MnTe/Bi_2Te_3$ monolayer with fifteen exchanged Mn-Bi pairs (F15) and the perfect $MnBi_2Te_4$ monolayer (F16) (all sixteen Mn-Bi pairs in $MnTe/Bi_2Te_3$ are exchanged) are chosen as IS and FS, respectively, with the kinetic barrier of 3.90 eV (**Fig. S3c**).

When vacancy of Bi (V_{Bi}) exists in the $MnTe/Bi_2Te_3$ monolayer, the Mn-Bi pair exchange is different from that in the perfect monolayer. Under this condition, the Mn-Bi pair exchange consists of two steps. One step is the migration of the neighbouring Mn atom to fill the V_{Bi} with the formation of V_{Mn} at the original Mn site, and another step is the migration of the neighboring Bi to fill the newly formed V_{Mn} with the formation of a new V_{Bi} near the previous V_{Bi}. As shown in **Fig. S4a**, in the initial stage, the $MnTe/Bi_2Te_3$ monolayer with V_{Bi} (I1-0) and with V_{Mn} (I1-1) are chosen as IS and FS for the migration of Mn, respectively, with a kinetic barrier of 1.07 eV. For the migration of Bi, the FS (I1-1) of the Mn migration, and the $MnTe/Bi_2Te_3$ monolayer with V_{Bi} and an exchanged Mn-Bi pair (I2-0) are chosen as IS and FS, respectively, with a kinetic barrier of 0.11 eV. The kinetic barriers of Mn migration and Bi migration in the middle stage are 0.97 eV and 0.60 eV, respectively (**Fig. S4b)**. In the final stage, the kinetic barriers of Mn migration and Bi migration are 1.05 eV and 0.99 eV,

respectively (**Fig. S4c**).

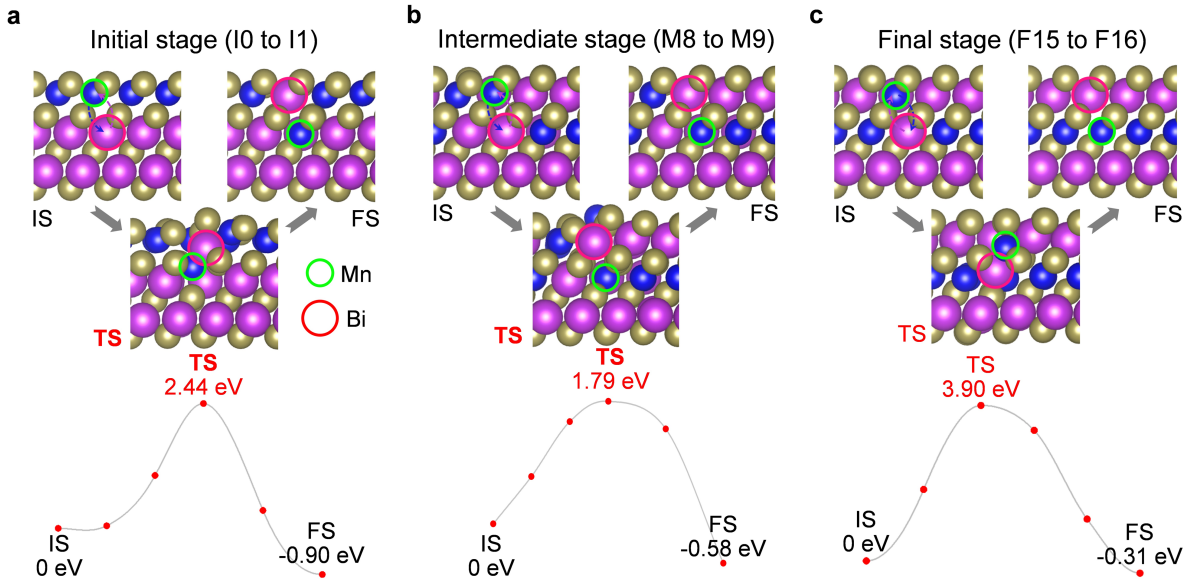

Figure S3. Energy profile of the Mn-Bi pair exchange during the phase transition from the perfect $MnTe/Bi_2Te_3$ to $MnBi_2Te_4$ monolayer. a Pair exchange in the initial stage, where none or a small number of Mn-Bi pairs complete the exchange. **b** Pair exchange in the intermediate stage, almost half of the Mn-Bi pairs complete the exchange. **c** Pair exchange in the final stage, where almost all Mn-Bi pairs complete the exchange.

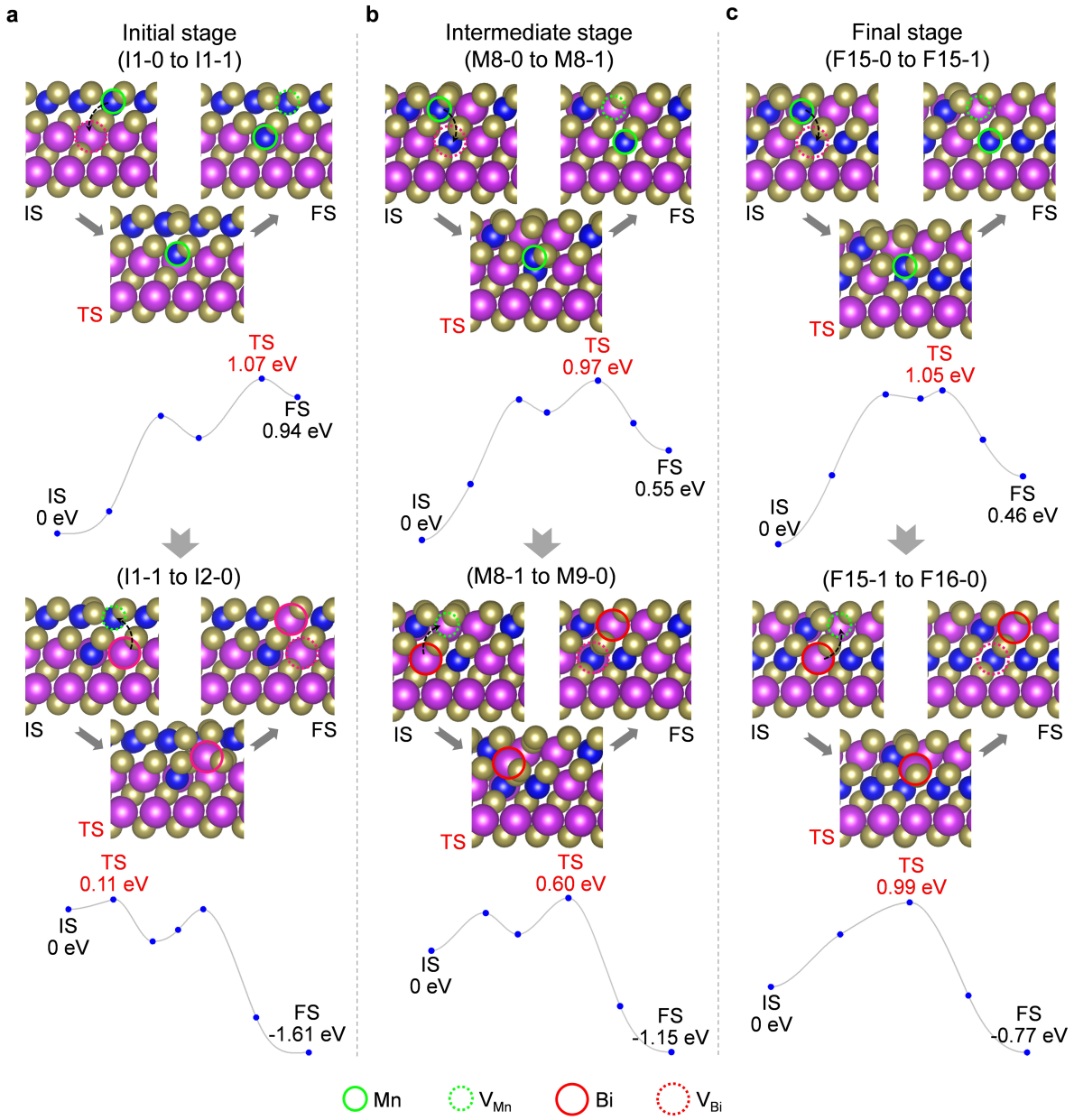

Figure S4. Energy profile of the Mn-Bi pair exchange during the phase transition from the $MnTe/Bi_2Te_3$ to $MnBi_2Te_4$ monolayer with V_{Bi} in $MnTe/Bi_2Te_3$. a Pair exchange in the initial stage, where none or a small number of Mn-Bi pairs complete the exchange. **b** Pair exchange in the intermediate stage, almost half of the Mn-Bi pairs complete the exchange. **c** Pair exchange in the final stage, where almost all Mn-Bi pairs complete the exchange.

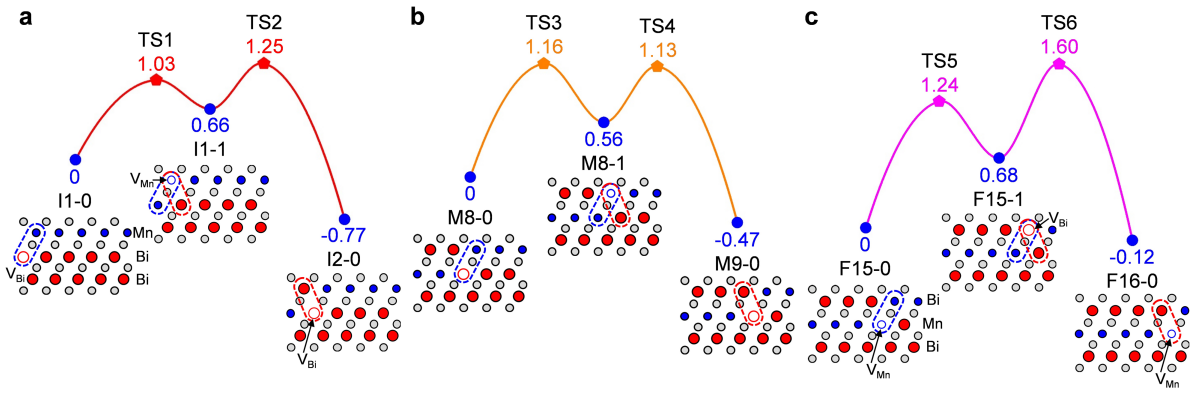

Fig. S5. Free energy profile of phase transition from the MnTe/Bi_2Te_3 to $MnBi_2Te_4$ monolayer in annealing temperature of 200 ℃. a Initial stage. **b** Intermediate stage. **c** Final stage. The blue, red and gray solid cycles refer to Mn, Bi and Te atoms, respectively. The blue and red hollow cycles refer to Mn and Bi vacancies (V_{Mn} and V_{Bi}), respectively. The blue dashed rounded-rectangles refer to the migration of Mn to Bi vacancy and the red dashed rounded-rectangles refer to the migration of Bi to Mn vacancy.

Tab. S1. Reaction energy and kinetic barrier of phase transition from the MnTe/Bi_2Te_3 to $MnBi_2Te_4$ monolayer with different annealing temperatures. T refers to annealing temperature, E_T refers to reaction energy, E_K refers to kinetic barrier.

Stage	T(200 ℃)		T(400 ℃)		T(600 ℃)	
	E_T (eV)	E_K (eV)	E_T (eV)	E_K (eV)	E_T (eV)	E_K (eV)
Initial	-0.77	1.25	-0.82	1.35	-0.88	1.45
Intermediate	-0.47	1.16	-0.42	1.28	-0.37	1.42
Final	-0.12	1.60	-0.05	1.69	0.01	1.78

Section IV. Band structures of $MnTe/Bi_2Te_3$ monolayer, $MnBi_2Te_4$ monolayer, and intermediates during the phase transition from the $MnTe/Bi_2Te_3$ to the $MnBi_2Te_4$ monolayer

In order to study the evolution of electronic properties in the phase transition process, the intermediates during the phase transition from the $MnTe/Bi_2Te_3$ to $MnBi_2Te_4$ monolayer are selected to calculate their band structures. There are five intermediates, including I1-0 and I2-0 in the initial stage, M8-0 in the intermediate stage, and F15-0 and F16-1 in the final stage. The band structures of the selected intermediates are summarized in **Fig. 3** and **Fig. S6**. Meanwhile, the band structures of the perfect $MnTe/Bi_2Te_3$ monolayer (Per-Ini) and the perfect $MnBi_2Te_4$ monolayer (Per-Fin) are also shown in **Fig. S6** for comparison to evaluate the effect of V_{Bi} on the Dirac cone. As shown in **Fig. S6**, the Dirac cone would open a gap as the amount of the exchanged Mn-Bi pairs increases during the phase transition from $MnTe/Bi_2Te_3$ to $MnBi_2Te_4$ monolayer.

The band structures of $MnTe/Bi_2Te_3$ and $MnBi_2Te_4$ monolayers with and without SOC are shown in **Fig. S7**. The SOC can shift the hole pocket upwards and the electron pocket downwards for the $MnBi_2Te_4$ monolayer, resulting in a reduction of the gap opening of the Dirac point-related bands (**Fig. S7a**). Such a shift of energy levels can also be observed in the metallic $MnTe/Bi_2Te_3$ monolayer (**Fig. S7b**).

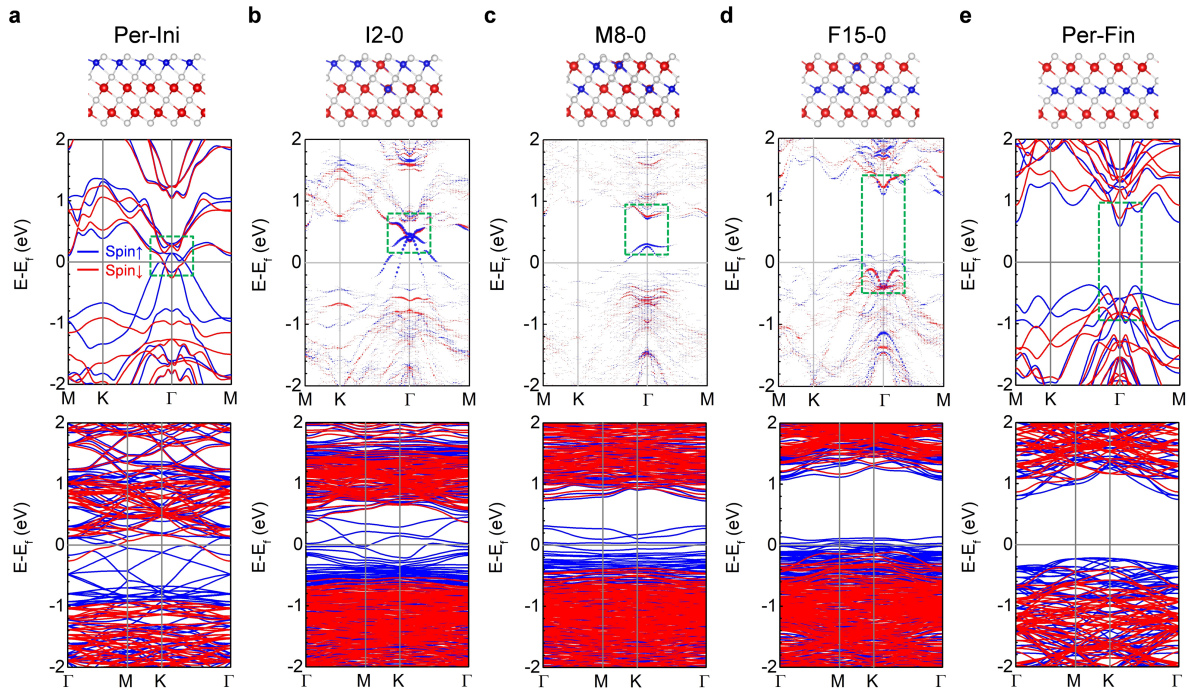

Figure S6. Band structure evolution during the phase transition from the MnTe/Bi_2Te_3 to $MnBi_2Te_4$ monolayer. a Band structures of the perfect MnTe/Bi_2Te_3 monolayer (Per-Ini) in primary unit cell and 4 × 4 × 1 supercell. **b, c, d** Unfolded and folded band structures of three intermediates in the initial stage (I2-0), intermediate stage (M8-0), and final stage (F15-0) during the phase transition of the lattice with V_{Bi} in MnTe/Bi_2Te_3. **e** Band structures of the perfect $MnBi_2Te_4$ monolayer (Per-Fin) in primary unit cell and 4 × 4 × 1 supercell. The green dashed squares mark the Dirac point-related bands.

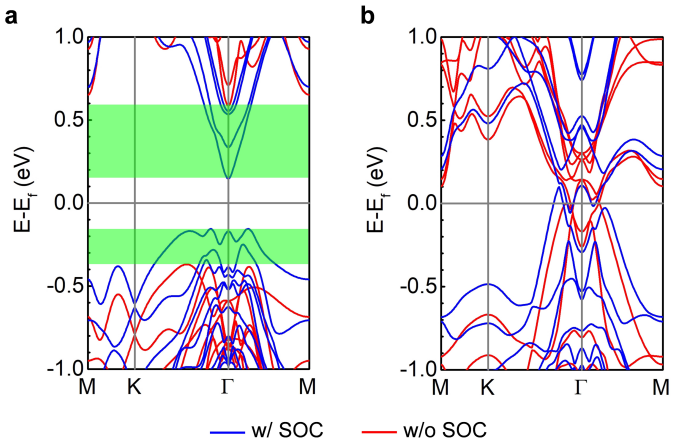

Figure S7 Band structures of $MnBi_2Te_4$ and MnTe/Bi_2Te_3 monolayer with and without spin-orbit coupling effect. a $MnBi_2Te_4$. **b** MnTe/Bi_2Te_3.

Reference:

[1] Kresse, G. & Furthmuller, J. Efficient iterative schemes for ab initio total-energy calculations using a plane-wave basis set. *Phys. Rev. B* **54**, 11169-11186 (1996).

[2] Blochl, P. E. Projector augmented-wave method. *Phys. Rev. B* **50**, 17953-17979 (1994).

[3] Kresse, G. & Joubert, D. From ultrasoft pseudopotentials to the projector augmented-wave method. *Phys. Rev. B* **59**, 1758-1775 (1999).

[4] Perdew, J. P., Burke, K. & Ernzerhof, M. Generalized gradient approximation made simple. *Phys. Rev. Lett*. **77**, 3865 (1996)

[5] Dudarev, S. L. et al. Electron-energy-loss spectra and the structural stability of nickel oxide: An LSDA+ U study. *Phys. Rev. B* **57**, 1505 (1998).

[6] Liu, C. et al. Robust axion insulator and Chern insulator phases in a two-dimensional antiferromagnetic topological insulator. *Nat. Mater.* **19**, 522-527 (2020).

[7] Li, J. et al. Intrinsic magnetic topological insulators in van der Waals layered $MnBi_2Te_4$-family materials. *Sci. Adv*. **5**, eaaw5685 (2019).

[8] Grimme, S., Antony, J., Ehrlich, S. & Krieg, H. A consistent and accurate ab initio parametrization of density functional dispersion correction (DFT-D) for the 94 elements H-Pu. *J. Chem. Phys.* **132**, 154104 (2010).

[9] Henkelman, G., Uberuaga, B. P. & Jonsson, H. A climbing image nudged elastic band method for finding saddle points and minimum energy paths. *J. Chem. Phys*. **113**, 9901-9904 (2000).

[10] Du, M. H., Yan, J., Cooper, V. R. & Eisenbach, M. Tuning Fermi levels in intrinsic antiferromagnetic topological insulators $MnBi_2Te_4$ and $MnBi_4Te_7$ by defect engineering and chemical doping. *Adv. Funct. Mater*. **31**, 202006516 (2020).

[11] Zeugner, A. et al. Chemical aspects of the candidate antiferromagnetic topological insulator $MnBi_2Te_4$. *Chem. Mater*. **31**, 2795-2806 (2019).